Vol. 08, No. 2 (2026) 1327-1334, doi: 10.24874/PES08.02B.021

Proceedings on Engineering Sciences

www.pesjournal.net

ARC-DISCHARGE METHODOLOGY: SYNTHESIS AND CHARACTERIZATION OF CARBON NANOTUBES

Oudjertli Salah [1]

Received 24.12.2025.
Revised 22.04.2026.
Accepted 14.05.2026.

Keywords:

CNTs, Electric Arc- Discharge, XRD, SEM, Optical Microscope

A B S T R A C T

Carbon nanotubes have a property combination that is difficult to ignore. A Young's modulus near 1 TPa, electrical behaviour that flips between metallic and semiconducting depending on how the sheet is rolled, thermal conductivity along the axis that matches diamond all packed into a cylinder a few nanometres wide. That combination is why they have stayed near the top of the research agenda in nanomaterials for thirty years, and why getting the synthesis right actually matters. We produced multi-walled carbon nanotubes by electric arc discharge. The reason for choosing this route over CVD or laser ablation is simple: no metal catalyst is needed, which removes the main contamination problem before it starts. Two graphite electrodes at 99.999% purity were mounted face-to-face inside a stainless-steel chamber filled with helium at sub-atmospheric pressure. A DC arc was struck between them, and the carbon sublimated from the anode recondensed on the cathode as a soot containing multi-walled nanotubes. Current, voltage, gap width, and helium pressure were all adjusted run by run until the discharge was stable and the cathodic deposit was consistently rich in nanotube material. The powder was then looked at three ways. XRD on a Rigaku Ultima IV with Cu-Kα radiation ($\lambda = 0.154056$ nm) gave the crystallographic picture: the (002) reflection sitting at $2\theta \approx 25.9°$, an interlayer spacing of 0.343 nm, and a mean crystallite size of 10.10 nm from the Debye–Scherrer equation. These numbers are exactly what you expect from well-graphitized multi-walled nanotube walls. SEM on an FEI Quanta 250 showed the morphology at higher resolution bifurcated and branched structures, outer diameters between 25 and 120 nm, agglomerated into the tangled mat that arc-discharge MWCNTs typically form. EDX found no metallic impurities. Optical microscopy on a NIKON ECLIPSE LV150N polarizing microscope then gave the mesoscale view: how the aggregates are sized and distributed across the powder, and how homogeneous the material looks at the scale relevant to processing. The three datasets fit together and tell a consistent story about what was made structural and compositional information that feeds directly into any subsequent work using these CNTs in nanoelectronics, polymer composites, or protective coatings.

[1] Corresponding author: Oudjertli Salah
Email: salah.oudjertli@gmail.com

1. INTRODUCTION

Carbon nanotubes (CNTs) represent one of the most extraordinary and extensively investigated classes of nanomaterials to have emerged from the broader field of carbon science. Since their landmark discovery by Iijima (1991), who first observed multi-walled carbon nanotubes (MWCNTs) in the cathodic deposits of an arc discharge experiment, these cylindrical carbon allotropes have captivated the scientific community and inspired an enormous body of research spanning materials science, condensed matter physics, chemistry, and biomedical engineering. At their structural core, carbon nanotubes are seamless cylinders formed by the helical rolling of one or more graphene sheets the celebrated single-atom-thick, hexagonally arranged carbon lattice that itself attracted unprecedented scientific attention following its isolation by Novoselov et al. (2004).

Structurally, CNTs are broadly classified into two principal categories: single-walled carbon nanotubes (SWCNTs), consisting of a solitary rolled graphene sheet with diameters typically in the range of 0.4–2.0 nm, and multi-walled carbon nanotubes (MWCNTs), comprising two or more concentrically nested graphene cylinders separated by an interlayer spacing of approximately 0.34 nm, closely approximating the interlayer distance observed in graphite (Dresselhaus et al., 1995). This structural distinction carries profound implications for the resulting physical properties. SWCNTs exhibit a higher degree of structural perfection and pronounced quantum confinement effects, rendering them particularly attractive for electronic applications, whereas MWCNTs offer superior mechanical robustness and are more amenable to large-scale production at competitive cost.

Carbon nanotubes are cylindrical carbon structures with diameters of only a few nanometers and lengths that may extend to several micrometers or even millimeters under optimized synthesis conditions. Mechanically, CNTs possess Young's moduli approaching 1 TPa and tensile strengths exceeding 60 GPa, surpassing conventional engineering steels by several orders of magnitude while maintaining a density approximately six times lower (Terrones, 2003). Electrically, depending on chirality and diameter, CNTs can behave either as metallic conductors or semiconductors with tunable bandgaps, a feature of immense importance for nanoelectronic device engineering (Dürkop et al., 2004; Hamada et al., 1992). Thermally, individual CNTs sustain conductivities exceeding 3000 $W \cdot m^{-1} \cdot K^{-1}$ along their axis, rivaling diamond and placing them among the most efficient heat-conducting materials known.

The remarkable combination of mechanical strength, electrical conductivity, thermal stability, and chemical versatility has positioned CNTs among the most promising materials for next-generation technologies. Their exceptionally high aspect ratio and large specific surface area provide unique opportunities for engineering multifunctional materials with properties unattainable using conventional constituents. In recent years, CNTs have been increasingly incorporated into advanced composite systems where they act simultaneously as structural reinforcements and conductive networks. Significant improvements in stiffness, fracture toughness, fatigue resistance, electrical conductivity, and thermal management have been reported in polymeric, ceramic, and metallic matrices reinforced with nanotubes. Such developments have generated substantial interest in sectors including aerospace engineering, transportation, renewable energy technologies, and high-performance structural materials. Beyond structural applications, CNTs have emerged as key components in numerous electronic and optoelectronic systems. Their ability to support ballistic electron transport and sustain extremely high current densities has stimulated extensive research into CNT-based transistors, nanoscale interconnects, field-emission devices, transparent conductive films, and flexible electronic platforms. As the miniaturization of conventional silicon technologies approaches fundamental physical limitations, carbon nanotubes are increasingly viewed as potential building blocks for future nanoelectronic architectures. Their compatibility with flexible substrates and their exceptional resistance to electromigration further enhance their attractiveness for emerging electronic technologies.

The scientific significance of carbon nanotubes extends well beyond engineering and electronics. Their unique surface chemistry and ability to undergo functionalization have enabled applications in environmental science, biotechnology, and medicine. Functionalized CNTs have demonstrated remarkable potential as carriers for targeted drug delivery, biosensing platforms, tissue-engineering scaffolds, and diagnostic imaging systems. In parallel, their large adsorption capacity and chemical stability have motivated investigations into water purification, pollutant removal, and environmental remediation technologies. Research has also demonstrated their effectiveness as highly sensitive sensors capable of detecting gases, biomolecules, and chemical contaminants at extremely low concentrations. These diverse applications continue to reinforce the strategic importance of CNTs within the broader framework of nanotechnology development.

Carbon nanotubes have many potential applications in electronics, medicine, composite materials, and catalysis. From a synthesis perspective, three principal methodologies have been established for the controlled production of CNTs: chemical vapor deposition (CVD), laser ablation, and electric arc discharge (Meyyappan, 2004). CVD, while highly versatile and suitable for large-scale production, frequently introduces structural defects and metallic catalyst residues that necessitate extensive post-synthesis purification. Laser ablation yields high-quality SWCNTs but demands expensive laser

infrastructure and offers limited scalability, restricting its widespread industrial implementation.
The electric arc discharge method was chosen as the method for the production of carbon nanotubes (CNTs), as it has several advantages over other methods of CNT production. It is a relatively simple and cost-effective method and can be used to produce a wide variety of nanotube morphologies. First demonstrated for nanotube production by Ebbesen and Ajayan (1992), the arc discharge technique exploits the intense localized heating generated between two graphite electrodes under an applied potential difference to sublimate carbon and recondense it into nanotubular architectures. The resulting CNTs typically exhibit a high degree of graphitic order, relatively few structural defects, and diameters spanning a wide range contingent upon the synthesis conditions employed (Journet et al., 1997; Bethune et al., 1993).

One of the most important advantages of arc-discharge synthesis lies in the exceptionally high temperatures generated within the plasma zone, often exceeding 3500 °C. Under these extreme thermodynamic conditions, carbon atoms vaporized from the graphite anode rapidly condense and reorganize into highly ordered graphitic structures. As a consequence, nanotubes produced by arc discharge frequently exhibit superior crystallinity compared with those synthesized by alternative techniques. The resulting graphitic ordering facilitates electron transport, enhances thermal conductivity, and improves mechanical integrity, all of which are desirable characteristics for advanced technological applications. Moreover, the absence or limited use of metallic catalysts minimizes contamination and simplifies subsequent characterization procedures.

Despite these advantages, the arc-discharge process remains highly sensitive to numerous operational parameters. Arc current, electrode separation distance, gas composition, operating pressure, cooling rate, and deposition geometry all exert significant influence on nanotube yield, diameter distribution, crystallinity, and purity. Optimizing these parameters remains an active area of investigation, as even small variations may substantially affect the morphology and structural quality of the synthesized material. Consequently, a detailed understanding of the relationship between synthesis conditions and nanotube characteristics remains essential for improving process reproducibility and facilitating future industrial implementation.

Research continues to improve synthesis methods, understand their properties, and develop applications for carbon nanotubes (Oudjertli et al., 2014). The characterization of as-synthesized CNT powders constitutes an indispensable step in validating structural integrity, assessing phase purity, and establishing structure–property relationships that ultimately govern performance in downstream applications. X-ray diffraction (XRD) provides crystallographic information including d-spacings, phase identification, lattice ordering, and mean crystallite dimensions (Cullity & Stock, 2001). Scanning electron microscopy (SEM) coupled with energy-dispersive X-ray spectroscopy (EDX) enables high-resolution morphological imaging alongside elemental compositional analysis. Optical microscopy (OM), while operating at coarser spatial resolution, furnishes valuable mesoscale information regarding aggregate morphology, particle distribution, and macroscopic homogeneity (Belin & Epron, 2005).

This research presents the elaboration of CNTs using the electric arc discharge method and their characterization through X-ray diffraction (XRD), scanning electron microscopy (SEM), energy-dispersive X-ray spectroscopy (EDX), and optical microscopy (OM). The primary objective is to establish a detailed and internally consistent picture of the structural, morphological, and compositional attributes of the produced CNT powder, with particular emphasis on the rigorous interpretation of characterization data in relation to established theoretical frameworks and published literature values. By integrating complementary characterization techniques operating across multiple length scales, this study seeks to contribute to the broader understanding of arc-discharge-produced carbon nanotubes and to further support their development for advanced applications in nanotechnology, nanoelectronics, energy storage systems, multifunctional composites, and emerging high-performance engineering materials.

2. SYNTHESIS OF CARBON NANOTUBES (EXPERIMENTAL PROCEDURE)

2.1 Materials and Reagents

Arc discharge was selected for this work because it produces CNTs without a metal catalyst, which keeps the material clean from the start. The carbon source was high-purity graphite (99.999%), approximately 40 g per run. Two electrodes were machined to the standard asymmetric geometry used in arc discharge CNT synthesis (Ebbesen & Ajayan, 1992; Journet et al., 1997): the anode was a solid graphite rod, 6 mm diameter and 100 mm long; the cathode was wider, 13 mm diameter and 40 mm long. The asymmetry matters the larger cathode surface area promotes stable cathodic deposition of the nanotube-bearing soot. Helium was used as the buffer gas rather than argon. Its higher thermal conductivity draws heat away from the arc zone more efficiently, which favours the growth of well-structured multi-walled nanotubes over disordered carbon (Colbert et al., 1994).

2.2 Arc Discharge Apparatus

The reaction chamber was a stainless-steel cylinder, 200 mm internal diameter and 300 mm tall, pumped down to pressures as low as 10^{-5} Torr by a rotary vane mechanical pump backed by a turbomolecular pump. Vacuum was

monitored by a Pirani gauge in the rough regime and a cold cathode ionization gauge at high vacuum. The two electrodes were held on independently adjustable feedthroughs with Teflon-sealed linear motion mechanisms, so the inter-electrode gap could be controlled during the discharge without breaking vacuum. Arc current was supplied by a DC power supply rated 0–50 kV, 0–100 A. A Type K chromel–alumel thermocouple positioned near the arc zone fed a precision temperature controller for continuous thermal monitoring. CNT deposits were collected on water-cooled stainless steel and glass plates arranged circumferentially around the electrode assembly, at a distance chosen to maximize deposition of the fibrous cathodic soot while limiting accumulation of amorphous carbon and fullerene by-products.

2.3 Synthesis Procedure

Before each run, both electrodes were polished through successive grits of silicon carbide abrasive paper 320, then 600, then 1200 to give clean, smooth contact surfaces. They were then ultrasonically cleaned in analytical-grade isopropanol for 15 minutes and dried in an oven at 80°C for 2 hours before being mounted face-to-face in the chamber.

The chamber was pumped down over 45–60 minutes until the base pressure stabilised at approximately 10^{-5} Torr. Helium was then admitted through a precision mass flow controller until the pressure reached 500 Torr (≈66.7 kPa). That pressure was determined through prior runs to give the best balance between nanotube yield and suppression of soot and fullerene side products.

The arc was initiated by bringing the electrodes into brief contact and then withdrawing them to establish a stable plasma. Current was held at 80–100 A, voltage at 20–25 V, giving a mean arc power of roughly 2 kW. As the anode graphite was consumed, it was advanced incrementally to keep the inter-electrode gap constant and maintain stable cathodic deposition. Each run lasted 5–10 minutes. After extinguishing the arc, the chamber was left to cool under helium for 30 minutes before venting. The collected powder contained CNTs with diameters in the 25–120 nm range (Kane et al., 2020).

2.4 Characterization Instruments

XRD: Diffractograms were recorded on a Rigaku Ultima IV diffractometer with Cu-Kα radiation (λ = 0.154056 nm), scanning from 2θ = 10° to 80° in steps of 0.02° at $2°\cdot min^{-1}$, Bragg–Brentano θ/2θ geometry, tube set at 40 kV and 40 mA. Peak positions, intensities, and FWHM values were extracted by pseudo-Voigt profile fitting in the PDXL2 software suite. Phase identification used the ICDD PDF-2 database.

SEM-EDX. Morphological observations were made on an FEI Quanta 250 equipped with a tungsten filament and an EDX detector. Accelerating voltages of 5–20 kV were used with a working distance of 10–15 mm, secondary electron detection for surface topographic contrast. Before imaging, a ~5 nm Au–Pd coating was sputter-deposited on the powder specimens to prevent charge build-up. EDX spectra were acquired at 20 kV with beam current adjusted to give a detector dead time of 20–30%; elemental quantification used the ZAF matrix correction. Magnification ranged from ×500 to ×100,000.

Optical microscopy. A NIKON ECLIPSE LV150N upright polarizing microscope was used, fitted with long-working-distance objectives at ×5, ×10, ×20, ×50, and ×100. Images were captured with a 5-megapixel NIKON DS-Fi2 camera under both bright-field and cross-polarized illumination, using NIS-Elements software. Powder specimens were prepared by dispersing a small quantity on glass slides under a coverslip for transmitted-light observation; thicker deposits were examined in reflected-light mode. The two modes together gave information on both internal aggregate structure and surface reflectivity.

3. RESULTS AND DISCUSSION

3.1 X-Ray Diffraction Analysis

Figure 1 shows the XRD pattern of our CNT powder. We see four peaks: 7.6°, 25.9°, 42.8°, and 53.4°, assigned to the (001), (002), (100), and (004) planes respectively. Clean baseline, no extra phases, narrow reflections. The (002) peak at 25.9° is what we look at first in any CNT diffractogram. It is the graphene interlayer stacking reflection. From Bragg's law we get d_{002} = 0.343 nm slightly above the 0.3354 nm of bulk graphite. That small shift is normal for MWCNTs. Rolling a flat graphene sheet into a tube strains the lattice, and adjacent concentric walls never stack in perfect AB registry the way they do in graphite. So 0.343 nm is expected, not a problem. What matters more is the shape of the peak: sharp, symmetric, high intensity. That tells us the graphitic ordering runs over many repeat units the walls are well-crystallized. This is what arc discharge gives when it is working well (Hosseini et al., 2012; Saravanan et al., 2010; Zhu et al., 2002).

The (100) peak at 42.8° (d = 0.211 nm) comes from the in-plane hexagonal carbon lattice. It is present and well-resolved, which means the sp^2 bonding in the walls is intact. The (004) peak at 53.4° is the second-order harmonic of (002) it only appears when the stacking coherence is genuinely long-range. Its presence here is a good indicator of wall quality. The weak (001) reflection at 7.6° corresponds to a shallow graphene winding geometry; the other three come from steeper configurations.
We used the (002) peak to calculate crystallite size by the Debye–Scherrer equation (Cullity & Stock, 2001):

$$D = 0.94\,\lambda / \beta \cos\theta \qquad (1)$$

Here λ is the X-ray wavelength, β is the FWHM, θ is the Bragg angle. For MWCNTs this gives the coherent scattering domain perpendicular to the graphene planes essentially a measure of how many walls stack together coherently. We get D = 10.10 nm, consistent with the 5–50 concentric wall range and 10–100 nm outer diameters typical of arc-discharge MWCNTs (Andrews et al., 2002; Dresselhaus et al., 1995). Two things worth noting about the baseline: no metal oxide reflections, no broad amorphous hump underneath the peaks. We ran this synthesis without a metal catalyst, so contamination was not expected but you check anyway. The powder is graphitic carbon. That is all.

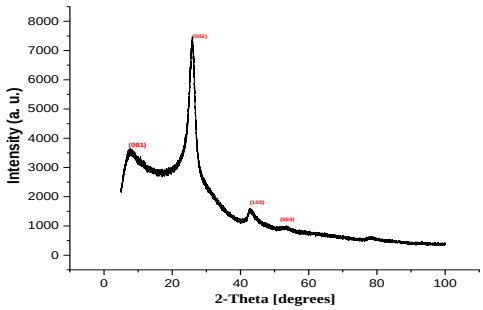

Figure 1. XRD patterns for as- produced CNTs by ar discharge method

3.2 Scanning Electron Microscopy (SEM) and EDX Analysis

SEM can be used to observe the morphology, size, and distribution of carbon nanotubes by arc-discharge method, and to identify impurities present in the carbon nanotubes. The micrographs obtained are presented in Figure 2 ((a), (b), (c), (d)) shows bifurcated and branched nanotubes with small-diameter secondary branches detaching from the wall of the primary nanotubes; also, particles of CNTs have spherical, ellipsoidal, and irregular shapes and are agglomerated.

At lower magnification, the powder presents as a dense, entangled fibrous matrix of high-aspect-ratio tubular entities with diameters spanning 25–120 nm and lengths extending to several micrometers, forming a characteristic "bird's nest" morphology commonly reported for arc discharge-derived MWCNTs (Ebbesen & Ajayan, 1992). The widespread entanglement and agglomeration of individual nanotubes into extended bundle networks are driven by strong van der Waals inter-tube adhesion forces one of the principal challenges in the processing and dispersion of CNT powders for composite fabrication.

The size of the particles of CNTs varies from a few nanometers to several micrometers.

At higher magnifications, bifurcated nanotubes exhibiting Y-junction morphologies and branched nanotubular architectures in which secondary branches of reduced diameter detach from the outer wall of primary nanotubes are clearly resolved. Such branched architectures arise from the incorporation of non-hexagonal carbon ring defects (pentagons and heptagons) into the graphene network during growth, which impose localized curvature enabling the topological continuity of the carbon network at junction points (Terrones, 2003). The observation of these features provides direct structural evidence for defect-mediated nanotube growth dynamics under the rapid cooling conditions of the arc discharge process.

Regarding the chemical composition, our SEM is coupled to an X-ray spectrometer to provide information on the elements that may be present in the carbon nanotube, see Figure 3.

The EDX spectrum exhibits a single dominant elemental signature at 0.277 keV corresponding to the C-Kα X-ray emission line of carbon, confirming that the synthesized material consists overwhelmingly of carbon with no detectable metallic catalyst impurities. This result is consistent with the catalyst-free arc discharge methodology employed and confirms the elemental purity of the produced CNT powder at the sensitivity limit of the EDX technique (~0.1–1 wt%). Any minor oxygen signal present is attributable to surface-adsorbed species during sample handling rather than to chemical contamination of the bulk nanotube material.

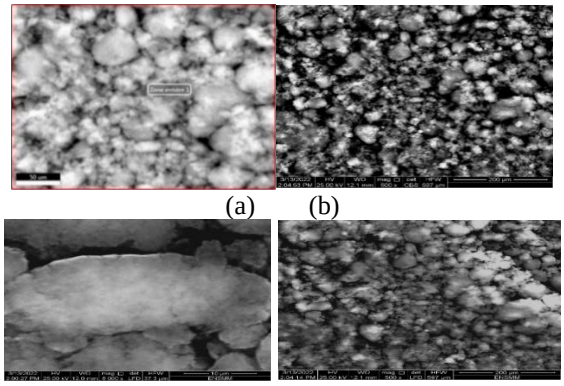

Figure 2. SEM micrograph of CNTs by arc-discharge method ((a,), (b), (c), (d))

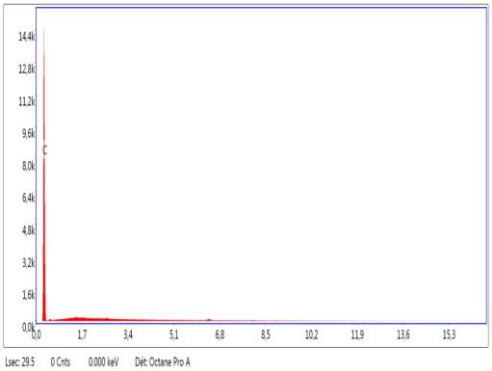

Figure 3. EDX analysis of CNTs by arc-discharge method

3.3 Influence of Chirality, Diameter, and Structural Factors on the Properties of Carbon Nanotubes

Theoretical calculations predicted that the carbon nanotube (Oudjertli, 2018) should have metallic or semiconductor behavior depending on their chirality and diameter (Dürkop et al., 2004). These conduction properties are inherited from the particular structure of the graphite tape. The graphene (Novoselov et al., 2004) sheet is a semiconductor band-gap zero: the valence band and conduction band meet precisely at the Fermi level at the six corners of the first Brillouin zone. The graphite should be metallic, but is in fact semi-metallic because its electron density at the Fermi level is very low.

The winding of a graphene sheet on itself creates periodic boundary conditions perpendicular to the axis of the nanotube. Therefore, a limited number of wave vectors is allowed in that direction (Hamada et al., 1992). It depends on the diameter and winding of the graphene sheet itself. If the boundary conditions include the corners of the Brillouin zone, the behavior of the nanotube is metallic. The electronic character of a CNT is governed principally by the chiral vector $C\_h = na_1 + ma_2$, where the integer pair (n, m) uniquely defines both the tube diameter and the winding angle (Saito et al., 1998). A CNT with indices satisfying $(n - m) \bmod 3 = 0$ exhibits metallic behavior; all other chiralities yield semiconducting nanotubes with bandgaps scaling inversely with diameter as $E\_g \approx 0.9$ eV/d(nm).

This is the case for all nanotube types, such as “chair,” and a third of nanotubes, such as “chiral” and “zig-zag” (Aoumeur, 2011). In other cases, the band structure has a band gap, in a first approximation, inversely proportional to the radius of the nanotube by the arc-discharge method. Metallic nanotubes have only two-dimensional conduction bands that cross the Fermi level; the full current flows through these two bands, and the theory predicts that the conductance ($G_0 = 2e^2/h$) equals twice the fundamental unit of conductance. The coherence length of conduction is significant and may reach the length of a nanotube ($> \mu m$). In addition to their high electrical conductivity, metallic nanotubes have excellent mechanical properties, such as high strength and stiffness, making them attractive for structural applications, such as nanocomposites and nanomechanical devices.

In addition to the chirality and diameter, the electronic properties of carbon nanotubes can be influenced by their length, their defects, and the nature of the contacts with the electrodes used for the measurements. Longer nanotubes have a higher resistance due to the increased probability of scattering events. Defects including Stone-Wales defect pairs, single- and multi-atom vacancies, and adatom-induced structural distortions introduce localized electronic states within the otherwise clean bandgap or at the Fermi level, modifying local density of states, charge scattering, and macroscopic conductivity. In the ballistic transport limit applicable to short, defect-free nanotubes, resistance is length-independent; in the diffusive regime characterizing longer or defect-rich nanotubes, resistance scales linearly with length due to elastic scattering at structural imperfections (Andrews et al., 2002). Strategies such as using metal nanoparticles or chemical functionalization can improve the quality of the contacts and reduce contact resistance.

3.4 Optical Microscopy Analysis

Using an optical microscope, we observed the morphology of the carbon nanotube using the arc-discharge method. In general, carbon nanotubes appear as a collection of black particles (Figure 4 (a), (b), (c), (d)). The particle size of carbon nanotubes varied from a few micrometers to several hundred micrometers. At low magnification (×50), the powder presents as a continuous field of optically opaque, deep-black particulate aggregates distributed against a lighter background the deep black coloration arising from the near-complete absorption of visible light across the entire spectral range, a direct consequence of the broadband electronic excitations available to the extended π-electron conjugation network of graphitic carbon (Belin & Epron, 2005).

Carbon nanotube particles have appeared in different forms, such as spheres, agglomerates, flakes, or fibers. The optical microscope allowed us to observe the homogeneous dispersion of carbon nanotubes and to evaluate their degree of purity. Furthermore, the micrographs show aggregates of carbon nanotubes that form clusters. Under higher magnifications (×100 to ×500), individual CNT agglomerates resolve into morphologically distinct entities: compact spheroidal clusters, elongated fibrous bundles, thin flake-like lamellar aggregates, and complex three-dimensional architectures formed by the interlocking and entanglement of primary nanotube bundles. Cross-polarized light observations reveal subtle birefringence contrast at the boundaries of larger crystalline aggregates, providing additional evidence for the locally anisotropic nature of the graphitic ordering within CNT bundles.

Regarding texture, the micrographs show variations in color and brightness on the surface of the carbon nanotube. These variations can be caused by differences in the orientation of the carbon nanotubes or by structural defects such as dislocations. Regarding granularity, the micrographs show variations in the size of the carbon nanotube aggregates. The spatial distribution of CNT aggregates across the sample surface is broadly homogeneous at the scale of the optical field of view (1–5 mm), attesting to the macroscopic uniformity of the arc discharge deposition and the powder collection procedures. Localized regions of coarser granularity characterized by particularly large (>100 μm) aggregates

are interspersed with zones of finer, more uniformly distributed particles, a textural heterogeneity attributable to the inherent variability in local cooling rates within different regions of the arc discharge plasma. Notably, the carbon nanotubes' granularity can significantly impact the properties of materials made from the powder. Finer granularity can improve the uniformity of material properties and mechanical strength, while coarser granularity can affect the electrical and thermal conductivity of the materials (Ajayan & Zhou, 2001).

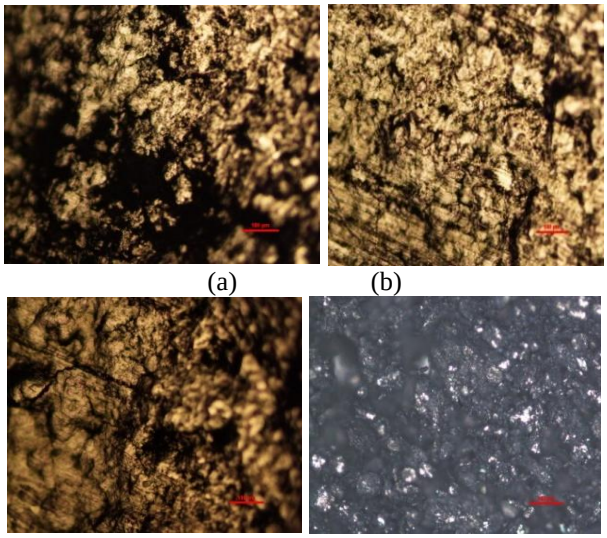

Figure 4. Optical microscope micrograph of CNTs by arc -discharge method ((a), (b), (c), (d)).

4. CONCLUSION

We used electric arc discharge to produce MWCNTs and characterized the powder by XRD, SEM-EDX, and optical microscopy. Here is what each technique gave us. XRD confirmed the graphitic structure. The (002) reflection sits at $2\theta \approx 25.9°$, giving an interlayer spacing of 0.343 nm consistent with multi-walled nanotube walls with the expected slight expansion relative to bulk graphite. Crystallite size from Debye–Scherrer is 10.10 nm, which fits the range reported for arc-discharge MWCNTs. The baseline is clean: no metal oxide peaks, no amorphous hump. The material is phase-pure graphitic carbon. SEM showed what the powder actually looks like at the nanoscale. Tubes with diameters between 25 and 120 nm, high aspect ratios, branched and bifurcated morphologies that point to defect-mediated growth during the arc process. The tubes agglomerate into the dense tangled networks typical of this synthesis route van der Waals forces between tube surfaces are strong enough that keeping them separated without functionalization is genuinely difficult. EDX found no metallic impurities. No catalyst was used, so this was the expected result, but it still needs to be verified rather than assumed.

Optical microscopy gave the picture at the scale between nanometers and millimeters aggregate size distribution, how the powder is spatially distributed, whether the material looks homogeneous at the scale relevant to mixing it into a composite or coating. That kind of information does not come from XRD or SEM.

Arc discharge is worth using for this. The graphite feedstock is cheap, the setup is not complicated, and the plasma temperatures reached above 3000°C are high enough to graphitize carbon into nanotubular structures without a metal catalyst. The trade-off is that dimensional control is limited and some amorphous carbon always ends up in the product. The obvious next steps are parameter optimization pressure, gas composition, arc current, inter-electrode gap, collector geometry to tighten the diameter distribution, and post-synthesis purification by acid treatment and thermal annealing to remove the amorphous fraction. With those improvements, these CNTs are relevant candidates for polymer nanocomposites, protective coatings, and nanoelectronic applications, where the combination of mechanical strength, conductivity, and chemical stability is directly useful.

References:

Ajayan, P. M., & Zhou, O. Z. (2001). Applications of carbon nanotubes. In M. S. Dresselhaus, G. Dresselhaus, & P. Avouris (Eds.), *Carbon nanotubes: Synthesis, structure, properties, and applications* (Topics in Applied Physics, Vol. 80, pp. 391–425). Springer. https://doi.org/10.1007/3-540-39947-X_14

Andrews, R., Jacques, D., Qian, D., & Rantell, T. (2002). Multiwall carbon nanotubes: Synthesis and application. *Accounts of Chemical Research*, *35*(12), 1008–1017. https://doi.org/10.1021/ar010151m

Aoumeur, B. (2011). *Thermal and electrical properties of carbon nanotube-based composites and application to gas sensing* [Doctoral thesis, University of Tlemcen]. University of Tlemcen, Algeria.

Belin, T., & Epron, F. (2005). Characterization methods of carbon nanotubes: A review. *Materials Science and Engineering B*, *119*(2), 105–118. https://doi.org/10.1016/j.mseb.2005.02.046

Bethune, D. S., Klang, C. H., de Vries, M. S., Gorman, G., Savoy, R., Vazquez, J., & Beyers, R. (1993). Cobalt-catalysed growth of carbon nanotubes with single-atomic-layer walls. *Nature*, *363*(6430), 605–607. https://doi.org/10.1038/363605a0

Colbert, D. T., Zhang, J., McClure, S. M., Nikolaev, P., Chen, Z., Hafner, J. H., ... & Smalley, R. E. (1994). Growth and sintering of fullerene nanotubes. *Science*, *266*(5188), 1218–1222. https://doi.org/10.1126/science.266.5188.1218

Cullity, B. D., & Stock, S. R. (2001). *Elements of X-ray diffraction* (3rd ed.). Prentice Hall.

Dresselhaus, M. S., Dresselhaus, G., & Saito, R. (1995). Physics of carbon nanotubes. *Carbon*, *33*(7), 883–891. https://doi.org/10.1016/0008-6223(95)00017-8

Dürkop, T., Getty, S. A., Cobas, E., & Fuhrer, M. S. (2004). Extraordinary mobility in semiconducting carbon nanotubes. *Nano Letters*, *4*(1), 35–39. https://doi.org/10.1021/nl034841q

Ebbesen, T. W., & Ajayan, P. M. (1992). Large-scale synthesis of carbon nanotubes. *Nature*, *358*(6383), 220–222. https://doi.org/10.1038/358220a0

Hamada, N., Sawada, S., & Oshiyama, A. (1992). New one-dimensional conductors: Graphitic microtubules. *Physical Review Letters*, *68*(10), 1579–1581. https://doi.org/10.1103/PhysRevLett.68.1579

Hosseini, A. A., Allahyari, M., & Besheli, S. D. (2012). Synthesis of carbon nanotubes, nanofibers and nanounions by electric arc discharge method. *International Journal of Science, Environment and Technology*, *1*(3), 217–229.

Iijima, S. (1991). Helical microtubules of graphitic carbon. *Nature*, *354*(6348), 56–58. https://doi.org/10.1038/354056a0

Journet, C., Maser, W. K., Bernier, P., Loiseau, A., Lamy de la Chapelle, M., Lefrant, S., ... & Fischer, J. E. (1997). Large-scale production of single-walled carbon nanotubes by the electric-arc technique. *Nature*, *388*(6644), 756–758. https://doi.org/10.1038/41972

Kane, A., Hinkov, I., Brinza, O., Hosni, M., Barry, A. H., Cherif, S. M., & Farhat, S. (2020). One-step synthesis of graphene, copper and zinc oxide graphene hybrids via arc discharge: Experiments and modeling. *Coatings*, *10*(4), 308. https://doi.org/10.3390/coatings10040308

Meyyappan, M. (Ed.). (2004). *Carbon nanotubes: Science and applications*. CRC Press. https://doi.org/10.1201/9780203494936

Novoselov, K. S., Geim, A. K., Morozov, S. V., Jiang, D., Zhang, Y., Dubonos, S. V., Grigorieva, I. V., & Firsov, A. A. (2004). Electric field effect in atomically thin carbon films. *Science*, *306*(5696), 666–669. https://doi.org/10.1126/science.1102896

Oudjertli, S. (2018). Electronic properties of carbon nanotubes. *Journal of Applied Material Science & Engineering Research*, *2*(1), 26–31.

Oudjertli, S., Bensalem, R., & Alleg, S. (2014). Different kinds of carbon nanotubes with their synthesis methods. In *Proceedings of the International Conference Nanotech MEET Tunisia 2014*.

Saito, R., Dresselhaus, G., & Dresselhaus, M. S. (1998). *Physical properties of carbon nanotubes*. Imperial College Press. https://doi.org/10.1142/p080

Saravanan, M. S. S., Babu, S. P. K., Sivaprasad, K., & Jagannatham, M. (2010). Techno-economics of carbon nanotubes produced by the open-air arc discharge method. *International Journal of Engineering, Science and Technology*, *2*(5), 100–108.

Terrones, M. (2003). Science and technology of the twenty-first century: Synthesis, properties, and applications of carbon nanotubes. *Annual Review of Materials Research*, *33*, 419–501. https://doi.org/10.1146/annurev.matsci.33.012802.100255

Zhu, H. W., Li, X. S., Jiang, B., Xu, C. L., Zhu, Y. F., Wu, D. H., & Chen, X. H. (2002). Formation of carbon nanotubes in water by the electric arc technique. *Chemical Physics Letters*, *366*(5–6), 664–669. https://doi.org/10.1016/S0009-2614(02)01658-6

Oudjertli Salah
Research Centre in Industrial Technologies.
(CRTI)
BP 64, Roade of Dely Brahim,
Cheraga 16014 Algiers,
Algeria
salah.oudjertli@gmail.com
ORCID 0000-0002-6707-7083